J. Fluid Mech. (1995), vol. 291, pp. 163–190



# Temporal analysis of capillary jet breakup

By N. ASHGRIZ AND F. MASHAYEK
Department of Mechanical and Aerospace Engineering, State University of New York at Buffalo, Buffalo, NY 14260, USA

(Received 15 November 1993 and in revised form 16 December 1994)

The temporal instability of a cylindrical capillary jet is analysed numerically for different liquid Reynolds numbers $Re$, disturbance wavenumbers $k$, and amplitudes $\epsilon_0$. The breakup mechanism of viscous liquid jets and the formation of satellite drops are described. The results show that the satellite size decreases with decreasing $Re$, and increasing $k$ and $\epsilon_0$. Marginal Reynolds numbers below which no satellite drops are formed are obtained for a large range of wavenumbers. The growth rates of the disturbances are calculated and compared with those from the linear theory. These results match for low-$Re$ jets, however as $Re$ is increased the results from the linear theory slightly overpredict those from the nonlinear analysis. (At the wavenumber of $k = 0.9$, the linear theory underpredicts the nonlinear results.) The breakup time is shown to decrease exponentially with increasing the amplitude of the disturbance. The cut-off wavenumber is shown to be strongly dependent on the amplitude of the initial disturbance for amplitudes larger than approximately $\frac{1}{3}$ of the initial jet radius. The stable oscillations of liquid jets are also investigated. The results indicate that liquid jets with $Re \sim O(1)$ do not oscillate, and the disturbances are overdamped. However, liquid jets with higher $Re$ oscillate with a period which depends on $Re$ and $\epsilon_0$. The period of the oscillation decreases with increasing $Re$ at small $\epsilon_0$; however, it increases with increasing $Re$ at large $\epsilon_0$. Marginal Reynolds numbers below which the disturbances are overdamped are obtained for a wide range of wavenumbers and $\epsilon_0 = 0.05$.

## 1. Introduction

A liquid jet issuing from a nozzle may break up into small drops when it is subjected to even minute disturbances. These disturbances can be in the form of surface displacement, pressure or velocity fluctuations in the supply system or on the jet surface, as well as fluctuations in liquid properties such as temperature, viscosity, or surface tension coefficient. In order to characterize the instability of a capillary jet, a harmonic disturbance is imposed on the surface of the jet and its growth rate is investigated. Such investigations have revealed that the jet is unstable for axial disturbances with wavenumbers less than a cut-off wavenumber $k_c$, and stable otherwise. For each wavelength of an unstable disturbance one main drop and one or more usually smaller drops, referred to as the satellite or spherous drops, are formed.

The main objectives of the studies on the liquid jet instability have been to obtain the growth rates of the initial disturbances (as a function of the disturbance wavenumber), the cut-off wavenumber, the drop sizes after the breakup, the breakup length, and the breakup time; and to determine the drop behaviour after the breakup (e.g. satellite merging), and effects of the initial disturbance amplitude, disturbance type (such as surface, pressure or velocity disturbances), initial velocity profile of the jet, and of the fluid properties. These studies have been both experimental and theoretical.

The experimental research on jet breakup dates back to the studies by Bidone (1829), Savart (1833), Magnus (1859), Plateau (1873), Boussinesq (1877), and Rayleigh (1882, 1896). These studies were aimed at understanding the mechanism of the jet breakup. The later experimental investigations focused on the determination of the breakup length and breakup time under various conditions (Smith & Moss 1917; Tyler & Watkin 1932; Tyler 1933). More quantitative experimental characterization of the jet breakup has been completed by Donnelly & Glaberson (1966) and Goedde & Yuen (1970) by studying the instability of a jet subject to a harmonic disturbance. They measured the amplitude variation along the jet and then calculated its growth rate. They showed that the linear theory well predicts the experimentally measured growth rates. Taub (1976) decomposed the measured amplitude of the disturbance into its harmonic components, and provided its variation along the jet axis. He showed that the nonlinear analysis of Yuen (1968) well predicts the growth along the axis of the fundamental and first two harmonic components. Rutland & Jameson (1970, 1971) measured the main and satellite drop sizes for various fluids. Pimbley & Lee (1977) investigated the formation of the satellite and its consequent merging. They obtained regions for backward, forward, and no merging of the satellites. Vassallo & Ashgriz (1991) investigated the breakup of a water jet at large disturbance wavelengths and for various disturbance amplitudes. They showed that the number of drops formed increased with increasing disturbance wavelength. They also studied the satellite merging as a function of disturbance amplitude. Others have studied the effects of the following: nozzle design (McCarthy & Molloy 1974); surrounding fluids (Crane, Birch & McCormack 1964, and Tjahjadi, Stone & Ottino 1992); fluid properties, such as the surface tension coefficient (Faidley & Panton 1990); superposition of several waves (Cline & Anthony 1978; Chaudhary & Maxworthy 1980*a*, *b*; Orme, Willis & Nguyen 1993; and Bousfield, Stockel & Nanivadekar 1990); slurry fluids (Ogg & Schetz 1984); and viscoelastic fluids (Kitamura, Mishima & Takahashi 1982; Kitamura & Takahashi 1982).

Theoretical investigation have been mainly through either perturbation-type analysis or one-dimensional models. These studies can be divided into two major categories, namely temporal and spatial analysis. In the temporal analysis, an infinite jet, stationary relative to a moving observer is considered and the growth rate of the disturbance amplitude along the jet is determined. In the spatial analysis, the growth rate of the disturbance amplitude along a semi-infinite jet is considered with the nozzle conditions fixed. Linear and nonlinear perturbation analysis or direct numerical methods are used in each category. A detailed review of these techniques up to 1979 is provided by Bogy (1979*b*) and will not be repeated here. However, different types of analysis are categorized and referenced in table 1. In this paper we consider the temporal instability of a viscous liquid jet; therefore, the remainder of the discussion is on this category of studies.

Rayleigh (1879) provided the first analytical description of the temporal instability of an inviscid incompressible jet using linear theory. He showed that an axisymmetric harmonic disturbance of the form

$$r = 1 + \epsilon_0 \exp(\omega t - ikz) \tag{1}$$

grows in time according to

$$\omega = \left[\frac{I_1(k)}{I_0(k)}(1-k^2)k\right]^{1/2}, \tag{2}$$

where $\omega$ is the growth rate, $\epsilon_0$ is the initial disturbance amplitude, $k$ is the disturbance wavenumber, and $I_0$ and $I_1$ are the modified Bessel functions of the first kind. In (1) and

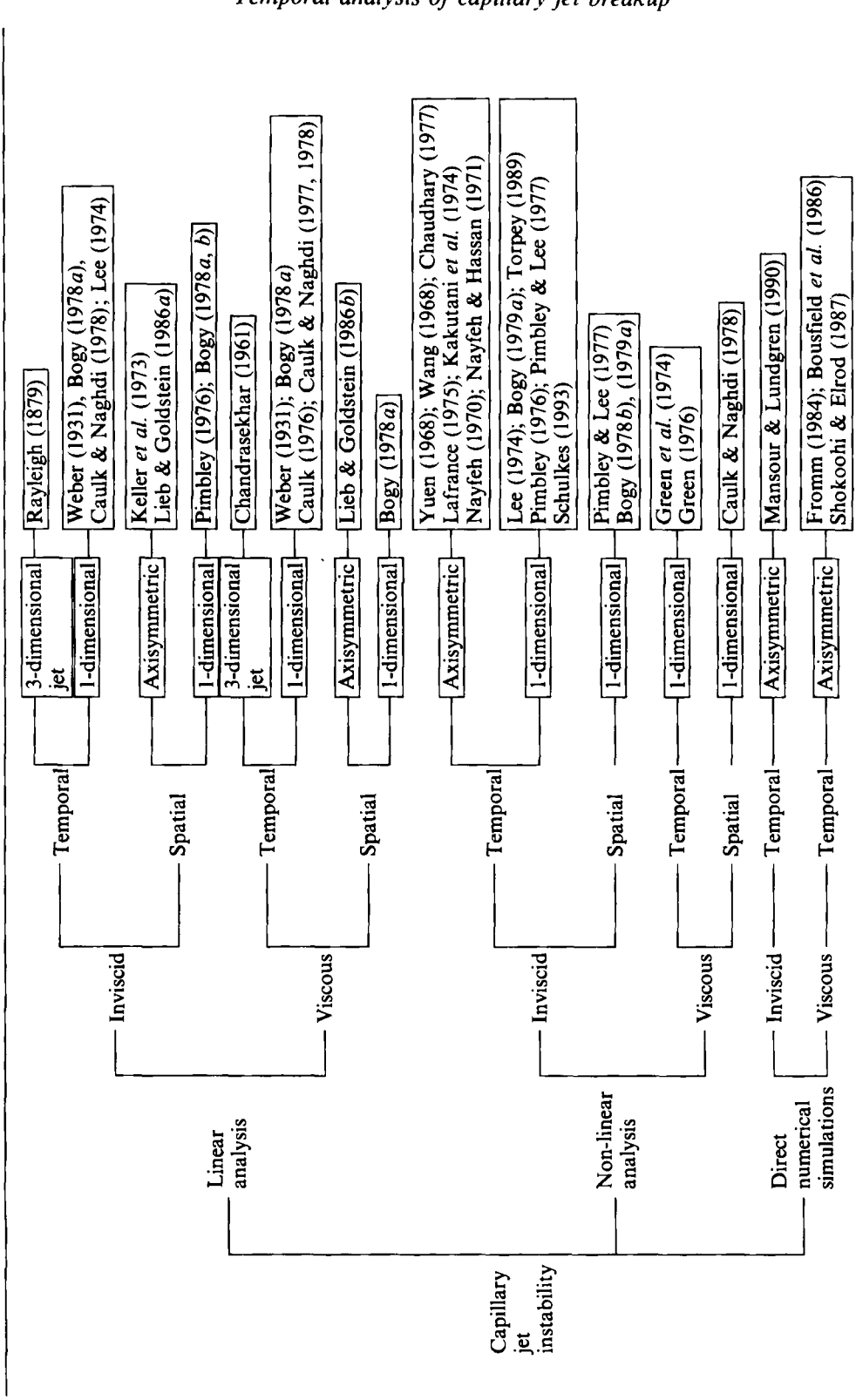


TABLE 1. Previous works on the capillary breakup of liquid jets.

(2), length and time variables have been non-dimensionalized by $r_0$ and $r_0/v_c$, where $v_c$ is the capillary-wave velocity $(\gamma/\rho r_0)^{1/2}$. Here, $r_0$ is the undisturbed radius of the jet, $\gamma$ is the liquid surface tension coefficient, $\rho$ is the density of the liquid. This result predicts that disturbances are unstable for $k < 1$ and stable for $k > 1$, i.e. the wavelength $\lambda = 2\pi r_0/k$ of the symmetrical deformation is less or greater than the circumference of the cylinder, respectively, and the maximum growth rate occurs at $k = 0.697$.

Later, Rayleigh's linear theory was extended by Yuen (1968), Nayfeh (1970), Lafrance (1975), and Chaudhary & Redekopp (1980) to include the nonlinear terms. The first attempt was by Yuen (1968) who showed that interaction occurred between harmonics of the disturbance, so that energy was extracted from the fundamental. His theory predicts that the neck (trough) of the wave shrinks faster than the swell (crest). However, at large times the theory also predicts that undulations occur in the neck between swells, that is, the jet exhibits more than one swell per wavelength. Nayfeh (1970) showed that this method leads to erroneous results near $k = 1$. Both the linear and nonlinear analysis of the jet instability, mentioned above, have considered the normal-mode type of analysis. Berger (1988) mentioned that the normal-mode analysis ignores the initial growth phase of the disturbances or perturbations to the basic state or flow. He treated the jet instability as an initial-value problem and after linearization showed that the growth of the instability is not exponential from initiation, as the normal-mode linear analysis predicts. Schulkes (1993) derived the complete one-dimensional equations governing the motion of an axisymmetric inviscid liquid jet. He solved his newly derived equations with proper boundary conditions numerically, and noted that as the disturbances grow, the characteristic axial lengthscales of the major feature became typically of the order of the radius of the jet. Therefore, the validity of the one-dimensional approximations for the investigations of the dynamics of the nonlinear liquid jet is questionable.

With the limitations and the problems associated with both the perturbation analysis and the one-dimensional models, it is of great interest to solve the full nonlinear equations numerically. Several attempts have been made in this direction. Fromm (1984) and Shokoohi & Elrod (1987) used a vorticity–stream function formulation to simulate the dynamics of a liquid jet. They demonstrated the validity of their methods by solving for the breakup of liquid jets with several different disturbance wavenumbers. Although the vorticity–stream function formulation can accurately track the liquid surface, it is computationally very intensive which inhibits a detailed study of the jet instability. Keunings (1986) developed a Galerkin finite element technique on deforming elements combined with a predictor–corrector scheme for the jet problem. Bousfield *et al.* (1986) compared the results of this technique with their one-dimensional thin-filament analysis, as well as the experimental results of Goedde & Yuen (1970). They were mainly concerned with the instability of viscoelastic jets and did not provide any detailed information on the breakup of Newtonian jets. Mansour & Lundgren (1990) used a boundary-integral method to study the instability of an inviscid jet. They calculated the main and satellite drop sizes as a function of the disturbance wavenumber. Their results agreed with the experimental data. Finally, Tjahjadi *et al.* (1992) investigated the breakup of a long liquid filament in a quiescent viscous fluid. They used a boundary-integral calculation to study the evolution of the filament as a function of the viscosity ratio of the fluids and the initial wavenumbers of the interface perturbation. They were mainly concerned with the subsequent breakup of the satellite drop into subsatellites.

A detailed numerical investigation of the breakup of a viscous liquid jet requires a very efficient and accurate numerical technique. One such technique is used here to

provide information on the dynamics of the capillary jets. In §§2 and 3 we describe the numerical technique. In §4 we discuss the mechanism of the jet breakup and address the jet behaviour in the vicinity of the cut-off wavenumber with respect to various parameters. In §5 we provide the first detailed analysis of the jet behaviour in the stable region, followed by concluding remarks in §6.

## 2. Mathematical and numerical formulation

An axisymmetric incompressible Newtonian liquid jet in vacuum and zero gravity is considered. The variables are non-dimensionalized by the radius of undisturbed jet $r_0$, and a characteristic time $(\rho r_0^3/\gamma)^{1/2}$. The dimensionless continuity and momentum equations are

$$\nabla \cdot \boldsymbol{u} = 0, \tag{3}$$

$$Re \frac{\mathrm{D}\boldsymbol{u}}{\mathrm{D}t} = \nabla \cdot \boldsymbol{T}, \tag{4}$$

where $\boldsymbol{u} = (u, v)$ is the velocity vector (see figure 1) and $\boldsymbol{T} = -p\boldsymbol{I} + [\nabla \boldsymbol{u} + (\nabla \boldsymbol{u})^T]$ is the stress tensor for Newtonian fluid. $\mathrm{D}/\mathrm{D}t$ is the total derivative operator defined as $\mathrm{D}/\mathrm{D}t = \partial/\partial t + \boldsymbol{u} \cdot \nabla$. In (4) the Reynolds number is defined based on the fluid properties and the initial jet radius: $Re = (1/\nu)(\gamma r_0/\rho)^{1/2}$, where $\nu$ is the kinematic viscosity. The stress balance on the free surface provides the following boundary condition, assuming the ambient pressure as the datum:

$$\boldsymbol{T} \cdot \boldsymbol{n} = Re\, K \boldsymbol{n} \quad \text{on the free surface,} \tag{5}$$

where $\boldsymbol{n}$ is the outward unit normal and $K$ is the curvature of the surface. We assume that the free surface can be represented by a height function $h(z, t)$, as shown in figure 1. Therefore, $K$ is given by

$$K = \frac{h_{zz}}{(1+h_z^2)^{3/2}} - \frac{1}{h(1+h_z^2)^{1/2}}. \tag{6}$$

Since a temporal analysis is considered here, the symmetry boundary conditions will apply on the axis of symmetry and planes of $z = 0$ and $z = \lambda/2$:

$$\frac{\partial u}{\partial r} = 0, \quad v = 0 \quad \text{at} \quad r = 0, \tag{7}$$

$$u = 0, \quad \frac{\partial v}{\partial z} = 0 \quad \text{at} \quad z = 0, \lambda/2, \tag{8}$$

where $\lambda$ is the disturbance wavelength. A Galerkin finite-element method with penalty function formulation is used to solve (3) and (4). Here the pressure is eliminated from the set of unknown variables by absorbing the continuity equation into the momentum equation (Hughes, Liu & Brooks 1979). In this formulation the pressure is defined as

$$p = -\Upsilon \nabla \cdot \boldsymbol{u}, \tag{9}$$

where $\Upsilon$ is a large number $O(10^9)$ depending on $\mu$ and $Re$. Four-node bilinear isoparametric elements are used to approximate the velocity distribution over each element:

$$\boldsymbol{u}(z, r, t) = \sum_{i=1}^{4} \boldsymbol{u}_i(t)\, N_i(z, r, t). \tag{10}$$

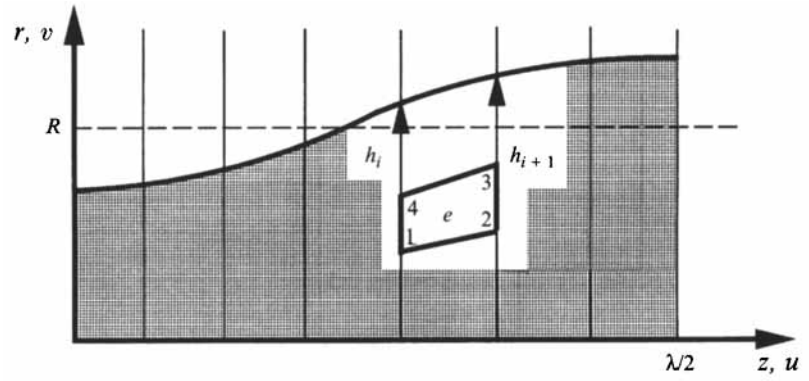


FIGURE 1. The fluid zone divided into subvolumes represented by their height and thickness.

A moving mesh is considered to discretize the computational domain. Therefore, the shape functions are time dependent. In order to obtain the finite-element formulation, (4) is multiplied by the shape function $N_j$, and integration is carried over the element volume. After the divergence theorem is invoked the resulting equation is

$$\int_{\Omega(t)} \left( N_j Re \frac{\mathrm{D}\boldsymbol{u}}{\mathrm{D}t} + \nabla N_j^T \cdot [-p\boldsymbol{I} + [\nabla \boldsymbol{u} + (\nabla \boldsymbol{u})^T]] \right) \mathrm{d}\Omega = \int_{\Gamma(t)} N_j \boldsymbol{T} \cdot \boldsymbol{n} \, \mathrm{d}\Gamma, \tag{11}$$

where $\Omega$ and $\Gamma$ are the volume and the surface area of the element, respectively. Substitution of (5) and (9) in (11) gives the following closed-form finite-element formulation:

$$\int_{\Omega(t)} \left( N_j Re \frac{\mathrm{D}\boldsymbol{u}}{\mathrm{D}t} + \nabla N_j^T \cdot [\Upsilon(\nabla \cdot \boldsymbol{u})\boldsymbol{I} + [\nabla \boldsymbol{u} + (\nabla \boldsymbol{u})^T]] \right) \mathrm{d}\Omega = \int_{\Gamma(t)} N_j Re \, Kn \boldsymbol{n} \, \mathrm{d}\Gamma. \tag{12}$$

The above formulation is based on the Eulerian or fixed mesh where the locations of the nodes do not change with time. Special treatment of time derivatives is required when a moving grid is considered. Since the shape function is time dependent, the time derivative of velocity in discretized form becomes

$$\left. \frac{\partial \boldsymbol{u}}{\partial t} \right|_{z,r} = \sum_{i=1}^{4} \frac{\mathrm{d}\boldsymbol{u}_i}{\mathrm{d}t} N_i + \sum_{i=1}^{4} \boldsymbol{u}_i \left. \frac{\partial N_i}{\partial t} \right|_{z,r}. \tag{13}$$

The last term of (13) introduces a new convective term in (12). Here, we allow the motion of the nodes in the $r$-direction only according to the following simple rule:

$$z_i(t+\delta t) = z_i(t) = \text{constant}, \quad r_i(t+\delta t) = c r_i(t), \tag{14}$$

where the subscript $i$ refers to the node number, and $c = c(z, t)$ is a constant for each column of nodes in the radial direction defined as

$$c = h(z, t+\delta t)/h(z, t). \tag{15}$$

Mashayek & Ashgriz (1993) have shown that the total derivative of the velocity in this case becomes

$$\frac{\mathrm{D}\boldsymbol{u}}{\mathrm{D}t} = \frac{\partial \boldsymbol{u}}{\partial t} + u \frac{\partial \boldsymbol{u}}{\partial z} + \left( v - \frac{c-1}{\delta t} r \right) \frac{\partial \boldsymbol{u}}{\partial r}. \tag{16}$$

Substitution of $\mathrm{D}\boldsymbol{u}/\mathrm{D}t$ from (16) into (12) concludes the finite-element formulation of the problem. More details are given in Mashayek & Ashgriz (1993).

| Wavenumber | 0.2 | 0.3 | 0.45 | 0.6 | 0.7 | 0.8 | 0.9 |
|---|---|---|---|---|---|---|---|
| Number of elements | 90 | 80 | 60 | 60 | 50 | 40 | 40 |

TABLE 2. Number of axial elements used in simulations for different wavenumbers

## 3. Free-surface determination

The free surface of the jet is unknown *a priori*, and is determined using the height-flux method (HFM) developed by Mashayek & Ashgriz (1993). Consider the liquid domain shown in figure 1 with a free surface at the top. We divide this domain into several vertical subvolumes of width $\delta z_I$ and volume $V_I$. The location of the free surface on the left and right sides of this subvolume is given by $h_i$ and $h_{i+1}$ at time $t$, respectively. Knowing the velocity distributions over the sideplanes, we find the location of the free surface, i.e. $h_i$ and $h_{i+1}$, at time $t+\delta t$. This is achieved by first calculating the net flux of the fluid passing through the sideplanes during the time interval $\delta t$, and determining the new volume of fluid, at $t+\delta t$, in the subvolume by adding the net flux to the previous volume at time $t$. Then, we assume that the part of interface which is located in any two neighbouring subvolumes can be approximated by a line segment defined by $h = az+b$, where $a$ and $b$ are two constants to be determined from the known volumes.

Details of this technique are given in Mashayek & Ashgriz (1993) and it is summarized below. The initial fluid domain is discretized into several (40–90) subvolumes and the volume of fluid in each subvolume is calculated. Then, the free surface is recovered from this set of numbers (subvolumes) using the line segment approximation. A finite-element mesh is then generated based on the free surface. The flow equations are solved and the velocity field is calculated. The new subvolumes are then found by calculating the flux of the fluid passing through the sideplanes. In the final step, the new free surface is reconstructed based on these numbers, and the new finite-element mesh is generated. This completes the sequence of operations needed to advect and reconstruct the fluid surface.

Numerical simulations were performed using four elements in the radial direction. The number of elements in the axial direction was changed based on the wavenumber as given in table 2. The nodes were equally spaced in the axial direction. However, in the radial direction the node spacing was changed owing to the surface deformation. The appropriate mesh for each case was found by performing computations using meshes of different resolutions. In general, the mesh implemented for any particular simulation was chosen to be about 25% more refined than the finest mesh predicted by this procedure in order to assure accuracy. A sample case for wavenumber $k = 0.63$ at $Re = 10$ is given in Mashayek & Ashgriz (1993) indicating that 40 elements in the axial direction provides acceptable accuracy for this wavenumber. However, the number of elements used in the axial direction for $k = 0.6$ and the same $Re$ was 60, which was well above the required limit. A similar procedure was utilized for mesh selection to study the oscillation of liquid jets in the stable region. Comparisons made throughout this work with other existing solutions are also useful to assess the accuracy of the calculations.

## 4. Temporal instability of capillary jets

Consider an infinitely long cylindrical Newtonian liquid jet, initially at rest with a spatially harmonic surface displacement of a cosine shape:

$$r = R - \epsilon_0 \cos(kz). \tag{17}$$

Here, $k = 2\pi R/\lambda$ and $R$ is determined such that the volume of the jet is kept constant when the initial amplitude is changed. Therefore,

$$R = (1 - \tfrac{1}{2}\epsilon_0^2)^{1/2}. \tag{18}$$

Owing to the symmetry, only half a wavelength of a cosine function is considered. The trough of the initial surface is set at $z = 0$, and the crest at $z = \lambda/2$. Hereinafter, the 'initial' crest of the sinusoidal surface is referred to as the swell point and its trough is referred to as the neck point. The dynamics of this jet due to capillary forces is investigated for various values of initial disturbance wavenumber $k$, amplitude $\epsilon_0$, and jet Reynolds number $Re$. The cut-off wavenumber for different $\epsilon_0$ is identified and the jet dynamics in both stable and unstable regions is investigated. In the following discussion, first the dynamics of a liquid jet for disturbances with wavenumbers less than the cut-off wavenumber is presented, followed by a description of the jet dynamics in the stable region.

Details of the shape evolution of liquid jets with $Re = 200$, 10, and 0.1 and $k = 0.2$, 0.45, 0.7 and 0.9, are presented in figure 2. The calculations are stopped when the radius of the jet at its minimum point reaches 1% of the undisturbed jet radius, i.e. $0.01 r_0$. This point is defined as the breakup point. It is assumed that the main characteristics of the actual breakup point (e.g. breakup time and the breakup location) are not significantly different from the breakup point defined here. Figure 2 reveals the following characteristics for the breakup of a capillary jet. (i) The breakup point moves towards the swell point of the jet as the jet $Re$ increases. This results in the formation of a ligament in addition to the main drops. The ligament will eventually form a satellite drop. (If the ligament is long enough it may further break up into more smaller drops.) (ii) The length and diameter of the liquid ligament decrease with increasing wavenumber $k$, and, therefore, so does the satellite size. (iii) The diameter of the liquid ligament and the satellite size increase with increasing $Re$ at a constant wavenumber. (iv) Satellite formation is inhibited at low $Re$. (v) The breakup time decreases with increasing $Re$. More detailed descriptions of these characteristics are given next.

### 4.1. *Location of the breakup point*

The linear theory predicts that the breakup point is always at the neck (trough) of the initial disturbance. However, figure 2 clearly shows that the breakup point is closer to the swell points. In fact only for very small $Re$ ($Re = 0.1$) does the breakup occur at the neck point, and as $Re$ increases the breakup point moves away from the neck. For high-$Re$ jets the fluid convection is more rapid and the neck region becomes flat while the diameter of the swell region increases. This results in the formation of two distinct regions in the jet: the middle region, where the curvature in the $(r, z)$-plane is very small and resembles a liquid ligament; and the swell region, where the curvature in the $(r, z)$-plane is large. For $Re = 200$, these two distinct regions are seen at $t = 22.398$ in figure 2($a$). Similar features are observed in figure 2($e$) for $Re = 10$ at slightly later time, $t = 22.415$. As $Re$ is reduced to 0.1, the displacement of the liquid becomes more difficult. Therefore, the disturbances basically grow locally, resembling the linear

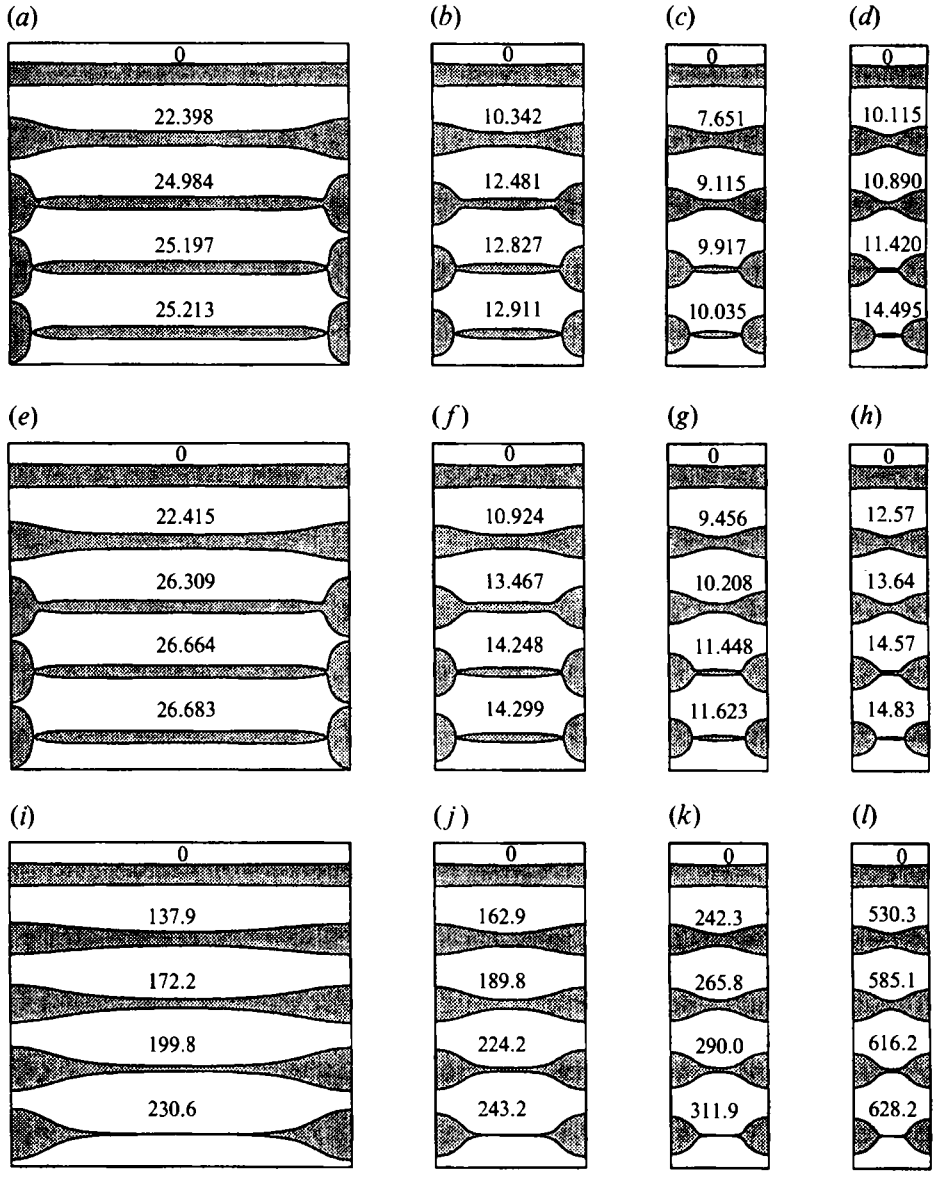


FIGURE 2. Time evolution of the instability of a capillary liquid jet, $\epsilon_0 = 0.05$: (*a*) $k = 0.2$, $Re = 200$; (*b*) $k = 0.45$, $Re = 200$; (*c*) $k = 0.7$, $Re = 200$; (*d*) $k = 0.9$, $Re = 200$; (*e*) $k = 0.2$, $Re = 10$; (*f*) $k = 0.45$, $Re = 10$; (*g*) $k = 0.7$, $Re = 10$; (*h*) $k = 0.9$, $Re = 10$; (*i*) $k = 0.2$, $Re = 0.1$; (*j*) $k = 0.45$, $Re = 0.1$; (*k*) $k = 0.7$, $Re = 0.1$; (*l*) $k = 0.9$, $Re = 0.1$. The numbers on the figures indicate the corresponding times.

theory. Figures 2(*i*)–2(*l*) show that the disturbances stay sinusoidal for very long time (relative to the breakup time) and may result in breakup of the jet at the neck point, $z = \lambda/2$. Generally, the liquid convection results in the diminishing of the surface curvature in the $(r, z)$-plane in the neck region and, consequently, the formation of the liquid ligament.

In order to gain better insight into the development of the breakup point of the jet, we have plotted the position of the minimum radius along the jet from $t = 0$ up to the

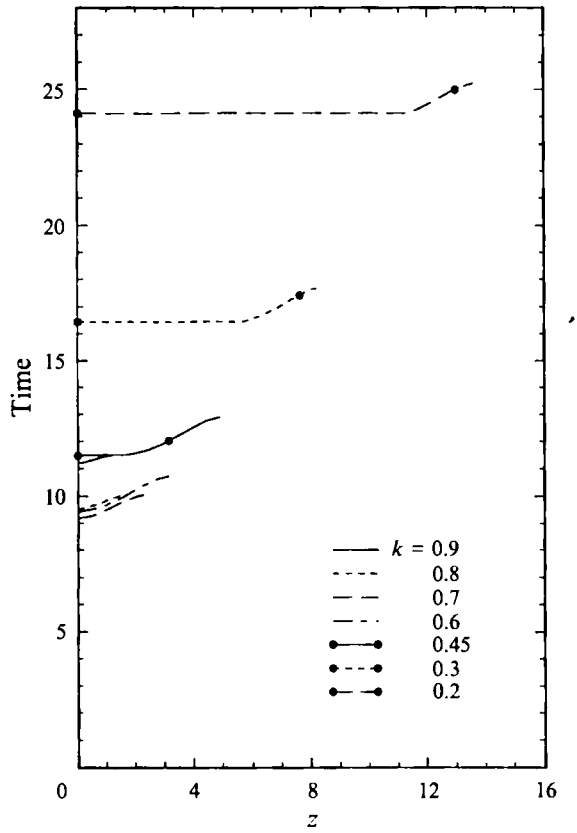


FIGURE 3. The motion of the location of the minimum radius of the jet along the jet axis.

breakup time, $t_b$. This plot is shown in figure 3 for a jet with $Re = 200$ and for $k = 0.2$, 0.3, 0.45, 0.6, 0.7, 0.8 and 0.9. Two different characteristic times are identified for each of the curves in this figure, the most important one being the time that the minimum point stays at $z = 0$. This time, $t_{b1}$, constitutes the greatest portion of the total breakup time and it first decreases and then increases with increase in the wavenumber. The minimum $t_{b1}$ occurs at the wavenumber for the maximum growth rate. Later, a flat region on each curve is observed which indicates a rapid displacement of the location of the minimum jet radius from the neck toward the swell points. This sudden relocation distance is longer for smaller wavenumbers and it is followed by a more gradual motion. The time of this gradual motion, $t_{b2}$, constitutes the second characteristic time for the jet breakup. During this time, which is much smaller than $t_{b1}$, the location of the minimum radius point of the jet continuously moves toward the swell point. The end points of the curves in figure 3 indicate the breakup times. One interesting feature to note is that the length of the slow moving part of the point of minimum radius remains approximately the same for all wavenumbers. Figure 3 shows that the breakup point moves closer to the swell point as the wavenumber is reduced. In other words, the ratio of the length of the ligament to the wavelength increases with decreasing wavenumber. The total relocation distance of the point of the minimum radius significantly decreases for low Reynolds number jets.

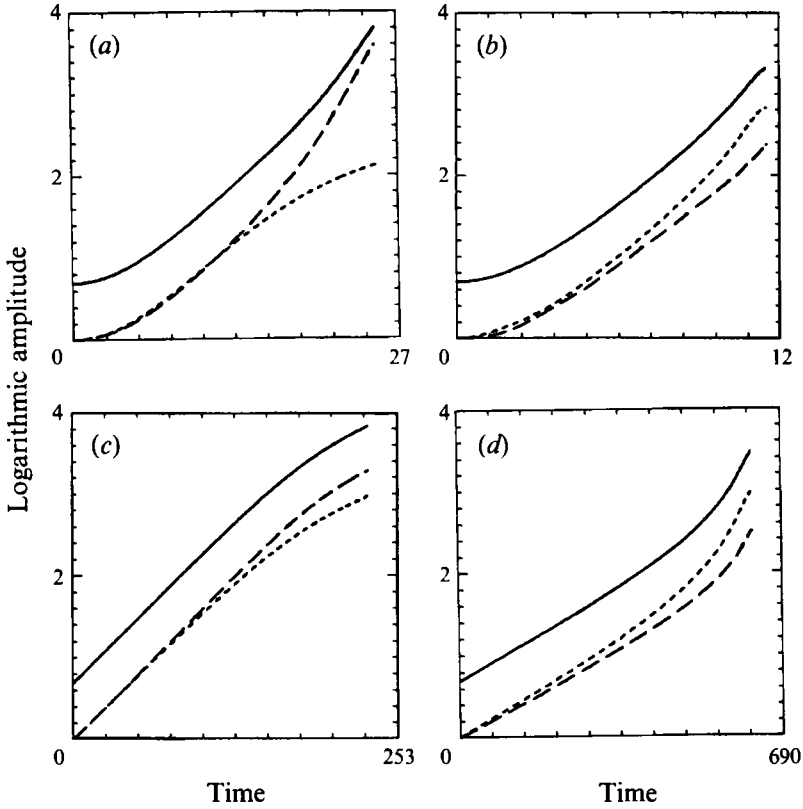


FIGURE 4. Variation of the amplitude of the swell (——), neck (---), and the difference between them (——) as a function of time; $\epsilon_0 = 0.05$: (*a*) $k = 0.2$, $Re = 200$; (*b*) $k = 0.9$, $Re = 200$; (*c*) $k = 0.2$, $Re = 0.1$; (*d*) $k = 0.9$, $Re = 0.1$.

### 4.2. *Growth rate of the disturbances*

The linear theory not only defines the region of unstable disturbance wavenumbers but also provides their growth rates. These growth rates are useful in estimating the breakup length and time. According to the linear theory the variation of the logarithmic value of the amplitude of the surface disturbances with time is linear. Although, for an actual liquid jet this amplitude variation may not be linear, the experimental results of Goedde & Yuen (1970) showed that for water and glycerin–water jets the logarithmic value of the difference between the amplitude at the neck and that at the swell varies linearly except close to the breakup time. They mentioned that the nonlinear effects at these two points cancel out. This cancelling effect has also been noted by Yuen (1968) who pointed out that the averaging process using the difference between swell and neck cancelled the second-order terms in his analysis. Goedde & Yuen (1970) plotted $\ln(A_s - A_n)$ as a function of time, where $A_s$ and $A_n$ are the amplitudes of the swell and the neck points in the jet. They used the linear region on this curve to describe a growth rate for each wavenumber.

Figure 4 shows the logarithmic values of the normalized amplitudes of the neck $((r_n - R)/\epsilon_0)$, the swell $((r_s - R)/\epsilon_0)$, and their difference $((r_s - r_n)/\epsilon_0)$ calculated by our full simulation for $Re = 200$, and 0.1, and $k = 0.2$ and 0.9. Here, $r_n$ and $r_s$ are the radii of the neck and the swell, respectively, and $R$ is given by (18). A single growth rate does not properly describe the actual behaviour of the jet. However, our nonlinear analysis

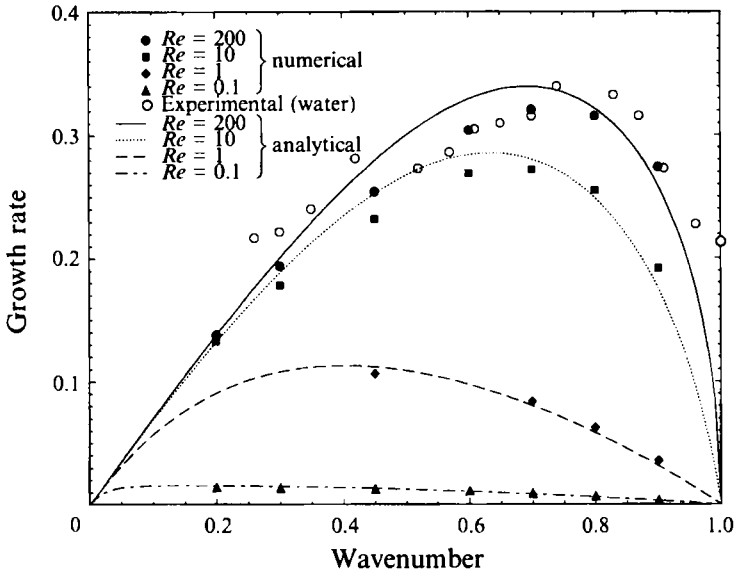


FIGURE 5. Comparison of the numerically calculated growth rates (symbols) with those from Chandrasekhar's linear theory and Cline & Anthony's (1978) experiment (○).

somewhat concurs with Goedde & Yuen's (1970) results, which showed that the logarithmic value of the difference between the neck and the swell may be approximated by a line, even though the logarithmic variation of the amplitude of the neck and the swell, by themselves, are not perfectly linear. In order to provide a value for the growth rate, a line is fitted to the difference between the amplitudes of the neck and swell and its slope is measured. The line is fitted only to the middle region of each curve, while the end regions are ignored. The dispersion curves are obtained using the calculated values of the growth rate for different wavenumbers and for four $Re$. The data are plotted in figure 5 along with the corresponding curves from Chandrasekhar's (1961) linear theory for a viscous jet. As predicted by the linear theory and observed experimentally, the viscosity reduces the magnitude of the growth rate for all wavenumbers. In addition, the maximum growth rate occurs at lower wavenumbers for more viscous jets. This is due to the more effective viscous damping at larger wavenumbers. The linear theory results in a better prediction for low-$Re$ jets. At high $Re$, the linear theory overpredicts the nonlinear growth rate for lower wavenumbers and underpredicts it at higher wavenumbers. The largest deviation at $Re = 200$ is approximately 10%. The experimental data of Cline & Anthony (1978) for water jets, which are also plotted in figure 5, show the same behaviour as the nonlinear results. However, the relatively large scatter observed in the experimental data reduces the possibility of one-to-one comparison.

Figure 4 reveals several other interesting features of the changes of the amplitudes of the neck and swell with respect to each other and as a function of time. Initially, the growth rate of the neck point is larger than the growth rate of the swell point, since a radial displacement in the neck region corresponds to a small radial displacement in the swell region for the same volume displacement. This can be seen for the short wavelengths (large $k$) of figures 4($b$) and 4($d$), where the neck amplitude seems to grow at a faster rate. For longer wavelengths, a longer ligament is formed and, consequently, a small decrease in the radius of the neck (or an increase in its amplitude) results in a

large decrease in the volume of the whole ligament. Therefore, after establishment of the ligament the growth rate of the amplitude of the neck decreases, eventually dropping below that of the swell. This relative change in growth rate is clearly seen in figures 4(*a*) and 4(*c*).

Close to the breakup point, the growth rate may increase or decrease depending on *Re* and *k*. For high-*Re* jets and small *k*, the growth rate of the neck point decreases close to the breakup time, while that of the swell point increases. This results in small variation of the growth rate of the difference between the two. On the other hand, for low-*Re* jets the growth rates of the neck and swell close to the breakup point both decrease for small *k* while they both increase for large *k*.

For the higher-*Re* jets of figures 4(*a*) and 4(*b*) an initially flat region on the amplitude curve is observed. This flat region has also been predicted by the initial-value analysis of Berger (1988) and observed experimentally by Chin (1983). The higher *Re*, the higher the initial flat region of the amplitude–time curve. It should be noted that for the initial disturbance amplitude of the present case the flat region can be as high as 10% of the breakup time. In other words, initially the disturbances may grow at a small rate for up to 10% of the total breakup time. Berger's (1988) initial-value analysis clearly shows that surface amplitude does not grow exponentially as $t \to 0$. He notes that as $t \to 0$ more and more modes become significant. Only after the higher modes are damped, does the single mode analysis takes effect and an exponential growth rate is observed. It may be possible to draw the same conclusion from figure 4. For the high-*Re* jets of figures 4(*a*) and 4(*b*) ($Re = 200$), a long initial period is observed before the surface amplitude assumes an exponential growth. However, for the low-*Re* jets of figures 4(*c*) and 4(*d*) ($Re = 0.1$), the higher harmonics damp out quickly and the surface amplitude assumes an exponential growth shortly after initiation.

To gain a better understanding of the effect of the nonlinearities on the jet breakup and the mode coupling, the jet surface shape is decomposed into its linear modes by implementing the Fourier expansion

$$r(z, t) = R + \sum_{n=0}^{\infty} c_n \cos(nkz). \tag{19}$$

The orthogonality of the cosine functions and numerical integration are used to determine the coefficients $c_n$. Figure 6 shows the amplitude of the fundamental, zeroth, second, third, and fourth harmonics of the initial disturbance with time corresponding to the cases given in figure 4. Figure 6(*a*) shows the fundamental and higher harmonics for a jet with $Re = 200$ and $k = 0.2$. Here, the second and third harmonics grow right from the initiation ($t = 0$). However, their amplitudes and growth rates are small in the beginning and become significant only later in time. In figure 6(*b*) for $Re = 200$ and $k = 0.9$, none of the harmonics grow until very close to the breakup time. It should be mentioned that a close inspection of the results reveals that the higher harmonics are present throughout the evolution of the jet (this is not observable in the scale shown here); however, they have a stable oscillatory behaviour with small amplitude of oscillation. The higher harmonics in this case do not grow until the formation of the thin ligament close to the breakup time.

The formation of the ligament can be explained by the nonlinear theories. The nonlinear analyses of Yuen (1968) and Chaudhary & Redekopp (1980) have revealed that the mode coupling results in a feedback from higher harmonics to the fundamental and vice versa. For instance, the second harmonic generates interactions between the first four harmonics only by considering the second-order solution. The modes

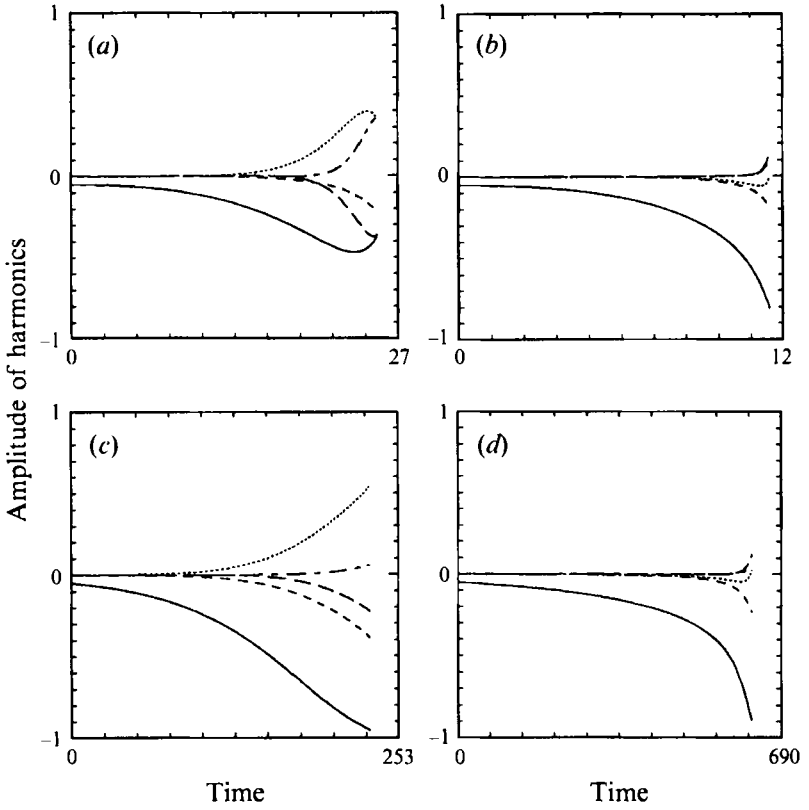


FIGURE 6. Amplitude of the fundamental (——), and zeroth (---), 2nd (· · ·), 3rd (—·—), and 4th (—··—) harmonics as a function of time; $\epsilon_0 = 0.05$: (*a*) $k = 0.2$, $Re = 200$; (*b*) $k = 0.9$, $Re = 200$; (*c*) $k = 0.2$, $Re = 0.1$; (*d*) $k = 0.9$, $Re = 0.1$.

generated by this coupling effect are not necessarily in phase with each other. Therefore, the second harmonic may generate a fundamental with a phase difference with the original fundamental disturbance. The summation of all of the fundamentals generated by this mode coupling results in the nonlinear variation of the fundamental, and the formation of the observed ligament. The growth rates of the disturbances on this ligament are different from the original jet, since their characteristic disturbance wavenumber, $k_l$, is less than $k$. The characteristic disturbance wavenumber for the ligament is defined as $k_l = 2\pi r_l/\lambda_l$, where $r_l$ and $\lambda_l$ are the characteristic radius and length of the ligament, respectively. Although $r_l$ and $\lambda_l$ are changing, the results indicate that, after the formation of the ligament, close to the breakup time $r_l/R < \lambda_l/\lambda$. Therefore, $k_l < k$ and the higher harmonics may grow if $nk_l < 1$. This explanation has to be contrasted with the weakly nonlinear solutions such as Chaudhary & Redekopp's (1980) third-order solution. They showed that if the fundamental input has a growing solution, all the harmonic components will have some growth associated with them, irrespective of whether or not their own wavenumber is below the cut-off. Based on our explanation, even if this feedback mechanism may result in very small growth rates for higher harmonics, in time the characteristic wavenumber decreases, strengthening the mode coupling and enhancing their growth rate.

As the wavenumber increases the higher harmonics do not grow until very close to the breakup time. In addition, for large wavenumbers the jet shape remains almost

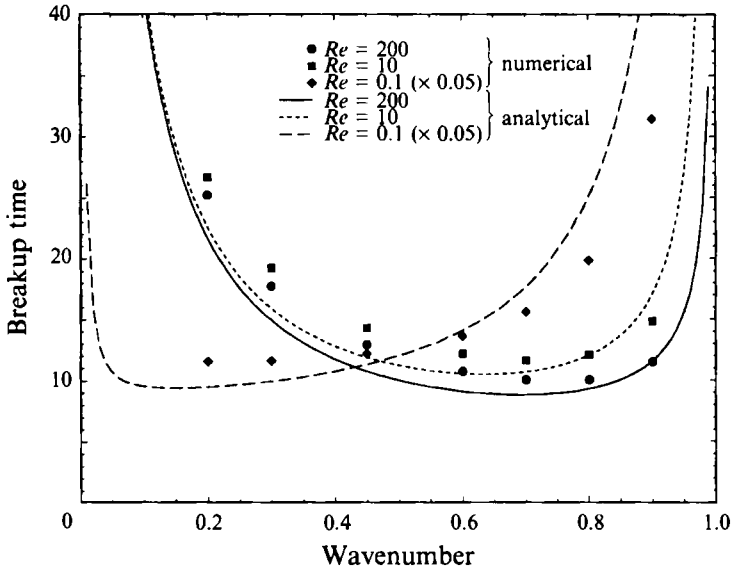


FIGURE 7. Comparison of the numerically calculated breakup times with $\epsilon_0 = 0.05$ (symbols) with those from Chandrasekhar's linear theory.

sinusoidal until the last moments of the breakup. This explains the rapid reduction of the ligament length with wavenumber. For smaller wavenumbers, the feedback mechanism from the higher harmonics to the fundamental seems to be small. In fact the energy is mainly transferred from the fundamental to the higher harmonics. Figure 6(*a*) shows a minimum in the amplitude of the fundamental. Here, significant energy is transferred from the fundamental to the second and third harmonics. Note that the signs of the second harmonic and the fundamental are different for smaller wavenumbers, but equal at larger wavenumbers. In addition, the study of the harmonics reveals that no significant changes with Reynolds number occur within the range $Re = 10$ to 200. Generally, the second harmonic contributes most to the observed nonlinearity in growth rates.

### 4.3. *The breakup time*

The breakup times for each wavenumber and for different $Re$ are shown in figure 7. The curves belong to Chandrasekhar's analytical solution where the breakup times are calculated from the growth rates using the relation $t_b = \ln(R/\epsilon_0)/\omega$. Our numerically calculated data are shown with symbols on figure 7 and are in good agreement with the analytical results only around the most unstable wavenumbers. For each $Re$, as the wavenumber increases the breakup time first decreases until it reaches a minimum and then increases. For $Re = 200$, the breakup time, $t_b$, decreases from 25.213 at $k = 0.2$ to a minimum of $t_b = 10.034$ at $k = 0.8$, and then increases to $t_b = 11.495$ at $k = 0.9$.

The breakup times for $Re = 10$ and 200 are not significantly different. However, as $Re$ decreases, the breakup time increases. The breakup time increases significantly on reducing $Re$ to 0.1. Here, although the jet is unstable, the growth of disturbances is very slow. The minimum breakup time occurs at lower wavenumbers as $Re$ decreases. This is in accordance with the linear theory.

It should be mentioned that the breakup time is significantly dependent on the initial disturbance amplitude. We have compared our results for the disturbance amplitude of $\epsilon_0 = 0.05$ with those of the linear theory, which are for infinitesimally small

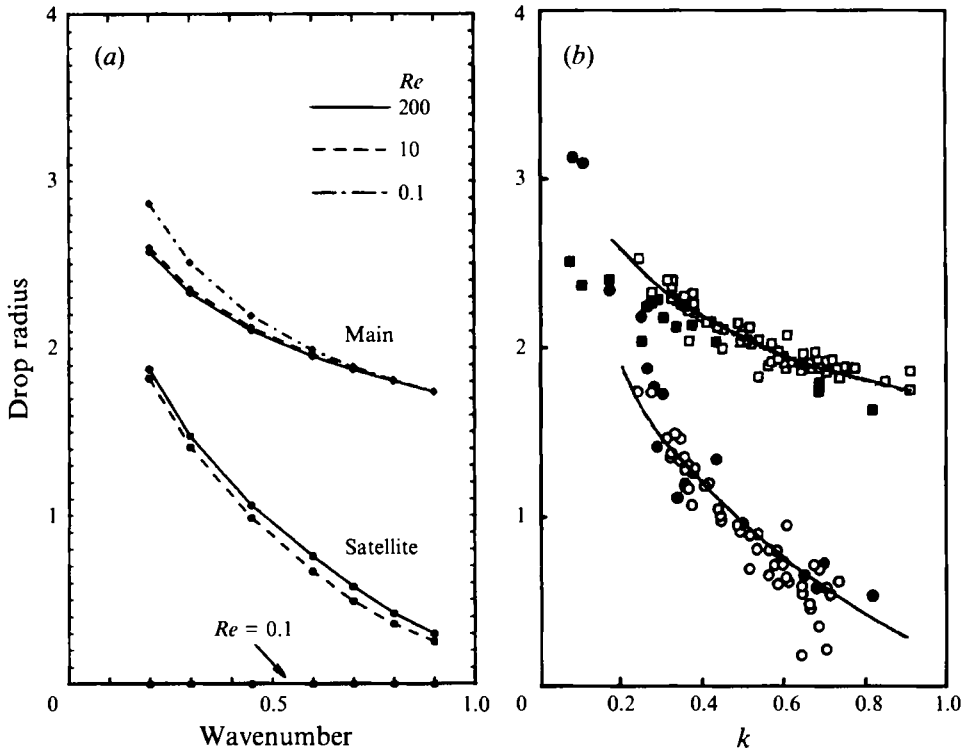


FIGURE 8. Variation of the main and satellite drop sizes with wavenumber: (*a*) effect of *Re*, (*b*) comparison with the experimental data of Rutland & Jameson (1970).

disturbance amplitudes. The reason that our nonlinear results compare well with those of the linear theory is that the small growth rates close to the initiation (as $t \to 0$) compensate for the large growth rates close to the breakup point. The initial-value analysis of Berger (1988) showed that the breakup times decrease from 0.75 to less than 0.5 of those of normal-mode analysis with *Re*. However, this reduction is due to the relatively large disturbance amplitudes in his calculation. In fact, since the initial-value analysis shows small initial growth rates, its breakup times should be larger than those of the normal-mode analysis, if very small initial amplitudes are used.

### 4.4. *Satellite size*

The first obvious deviation from the linear theory, as noted in §4.1, is the formation of a ligament between the main (parent) drops after the breakup. This ligament eventually becomes spherical and forms the satellite drop (it may also break into more smaller drops). Therefore, the volume of the ligament between the main drops after the breakup provides the satellite size. Figure 2 clearly shows that as the wavelength increases the length of the ligament and consequently the satellite size increase. Figure 8(*a*) shows the variation of the main drop radius as well as the radius of the satellite drop for different wavenumbers and for $Re = 0.1$, 10, and 200. Generally, for Reynolds numbers larger than 10 there is no significant change in size with *Re*. This explains the observed agreement between the results obtained by the inviscid theories (both weakly nonlinear analysis and boundary-integral calculations of full nonlinear equations) and the experimental data for water jets ($Re = 200$). However, for $Re < 10$ the variation becomes more pronounced. A comparison of our calculated drop and satellite sizes and

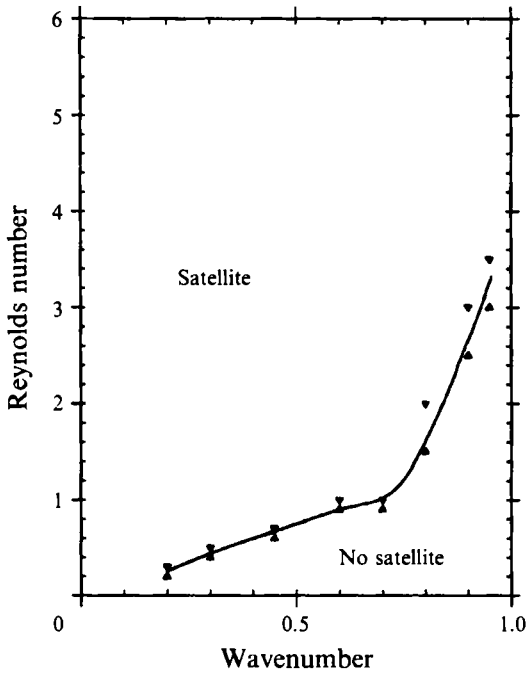


FIGURE 9. The satellite/no-satellite regions in the $(Re, k)$-domain: ▲, no satellite is formed; ▼, small satellite is formed.

the values measured by Rutland & Jameson (1970) is given in figure 8(*b*), which shows good agreement between the two.

The results show that for the same disturbance wavenumber the satellite size decreases with decreasing *Re*. Again, for low-*Re* jets, the viscous damping of the higher harmonics delays the movement of the minimum point and, consequently, results in a reduction of the ligament length. In addition, low-*Re* jets need a higher pressure difference between the ligament and the drop to overcome the dissipative and inhibiting effects of viscosity in order to cause detachment of the ligament from the drop. This latter effect results in the reduction of the ligament diameter. An increase in viscosity strengthens the fluid's inhibiting effects and in order for detachment to occur the ligament should become more slender and threadlike. The combined effects of reduced length and diameter of the ligament result in significant reduction of the satellite size for highly viscous liquids, as seen in figure 8(*a*).

Because of its practical importance, we have obtained the marginal jet Reynolds numbers, for a range of disturbance wavenumbers, below which no satellite is formed. Figure 9 shows the satellite/no-satellite regions in terms of *Re* and $k$ for $\epsilon_0 = 0.05$. For each wavenumber two data points are shown. The satellites are formed for the upper data point, and no satellite is obtained for the lower point. A curve is passed through these points to define the satellite/no-satellite regions. As *Re* is increased, satellite drops are eventually formed for all the unstable wavenumbers. An interesting observation made from figure 9 is that the slope of the limiting *Re* versus wavenumber curve changes significantly around $k = 0.7$. For $k < 0.7$ much smaller-*Re* jets are needed in order to prevent satellite drop formation. For $k > 0.7$ the slope of the curve is drastically increased and the limiting *Re* increases faster with the wavenumber.

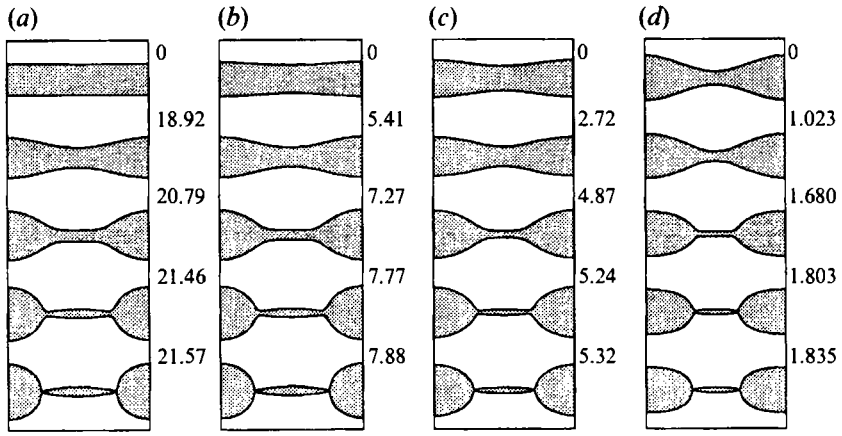


FIGURE 10. Effect of the amplitude of the initial disturbance on the breakup of the jet; $Re = 200$, and $k = 0.7$: (*a*) $\epsilon_0 = 0.001$, (*b*) $\epsilon_0 = 0.1$, (*c*) $\epsilon_0 = 0.2$, (*d*) $\epsilon_0 = 0.5$. The numbers on the figures indicate the corresponding times.

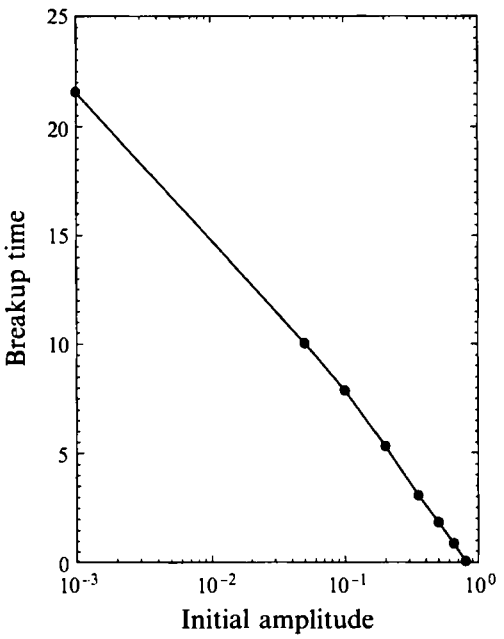


FIGURE 11. Variation of the breakup time as a function of the initial amplitude for $Re = 200$ and $k = 0.7$.

### 4.5. *Effect of disturbance amplitude*

The effects of large disturbance amplitudes on the breakup of a jet with $Re = 200$, and $k = 0.7$ are investigated. The results for initial disturbance amplitudes of $\epsilon_0 = 0.001$, 0.1, 0.2 and 0.5 are presented in figure 10. Note that since the volume is kept constant, the initial diameter of the neck decreases significantly as the initial disturbance amplitude is increased. Results indicate that the increase in the initial amplitude reduces the breakup time as shown in figure 11. These results confirm the logarithmic behaviour of the breakup time, which was derived by Chaudhary & Maxworthy (1980*a*), only for small amplitudes. However, as $\epsilon_0$ is increased a deviation from this logarithmic behaviour is observed.

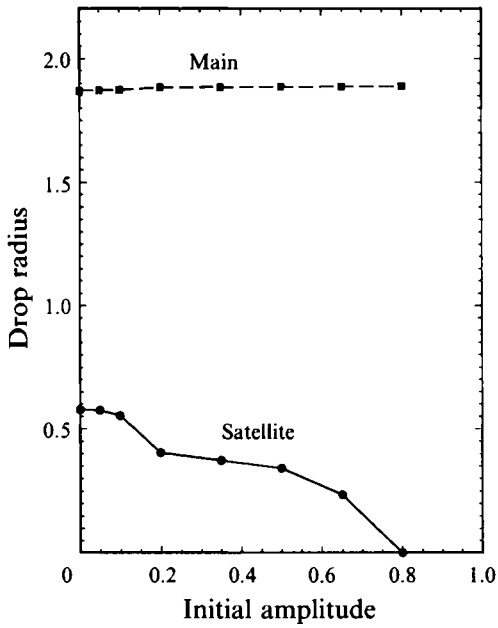


FIGURE 12. Variation of the main and satellite drop sizes as a function of the initial amplitude for $Re = 200$ and $k = 0.7$.

A plot of the main and satellite drop sizes as a function of initial disturbance amplitude is given in figure 12. The satellite size does not decrease monotonically with amplitude. At small initial amplitudes the satellite size does not change significantly. As the amplitude is further increased, a sharp change in the satellite size is observed at amplitude of around 0.2. This sudden change can be seen by comparing figures 10(*b*) and 10(*c*) for $\epsilon_0 = 0.1$ and 0.2, respectively. Note that the diameter of the ligament significantly decreases on increasing the amplitude from 0.1 to 0.2. However, after $\epsilon_0 = 0.2$ the ligament becomes small enough that its diameter does not decrease as fast. Only by increasing $\epsilon_0$ to 0.5 (figure 10*d*) can one see some decrease in ligament diameter and, consequently, a decrease in satellite size. After this point, the satellite size decreases monotonically with amplitude. The amplitude is increased until no satellite is formed. The results indicate that the satellite formation persists up to the point where the initial neck diameter is almost zero.

### 4.6. *Cut-off wavenumber*

Linear theories by Rayleigh (1879) for inviscid jets and Chandrasekhar (1961) for viscous jets predict that a jet is unstable for disturbances with wavenumbers smaller than 1 and stable for wavenumbers greater than 1. The cut-off wavenumber of $k_c = 1$ is found to exist in the limiting case of an infinitesimal initial disturbance. The nonlinear theories by Wang (1968) and Lafrance (1975) also predict $k_c = 1$. However, the nonlinear theories by Yuen (1968) and Nayfeh (1970) predict that the cut-off wavenumber varies with the initial disturbance amplitude as $k_c = 1 + (9/16)\epsilon_0^2$, and $k_c = 1 + (3/4)\epsilon_0^2$, respectively. Chaudhary's (1977) nonlinear analysis results in a transitional zone for the cut-off wavenumber based on the initial disturbance amplitude. His analysis shows that in the cut-off zone the growth rate changes from exponential to linear near $k = 1$ and finally to an oscillatory solution. Experimental results of Chaudhary & Maxworthy (1980*b*) have shown a linear growth rate for large

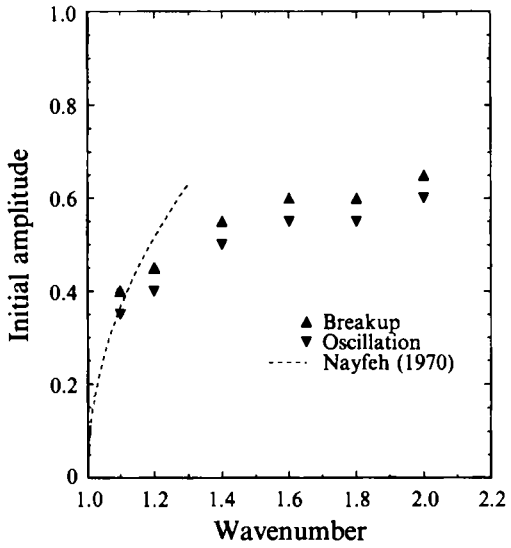


FIGURE 13. Effect of the amplitude of the initial disturbance in increasing the cut-off wavenumber for $Re = 200$. Numerical calculations (symbols) are compared with the analytical result of Nayfeh (1970).

initial inputs and transition towards a higher growth rate (i.e. smaller breakup time) for lower inputs near the cut-off wavenumber of 1.

The above analytical results are only valid for very small disturbances. We have carried out full simulations for a large initial disturbance amplitude for a jet with $Re = 200$. Figure 13 shows the cut-off wavenumbers as a function of the initial disturbance amplitude. The analytical results of Nayfeh (1970) are also plotted for comparison. The numerical simulations could not be extended to values of $k$ close to 1; therefore, close comparison with Nayfeh's equation is not possible. However, it can be said that Nayfeh's theory seems to work for $\epsilon_0$ up to 0.4. Our results indicate that in order to make the jet unstable above $k = 1$, the initial amplitude of the disturbance has to be increased significantly at first. However, after a certain amplitude, the jet becomes unstable for a large range of wavenumbers with only small increases in the amplitude. For instance, increasing $\epsilon_0$ from 0.01 to 0.35 will increase $k_c$ from 1 to 1.1; however, increasing $\epsilon_0$ from 0.35 to 0.5 will increase $k_c$ from 1.1 to 1.4.

## 5. Stable oscillation of capillary jets

Since all naturally observed capillary jets are unstable, the main objective of the studies in this area has been to understand the breakup mechanism. Therefore, less attention has been devoted to the understanding of the behaviour of the jet in the stable region. However, in §4, we have shown that any initial disturbance generates other disturbances on the jet. The newly generated disturbances or the higher harmonics may be stable if their wavenumber is larger than the cut-off wavenumber. Therefore, a better understanding of the behaviour of a capillary jet subject to disturbances with wavenumbers larger than the cut-off wavenumber (i.e. stable region) can help in explaining the influence of the higher harmonics on the jet instability and in designing disturbances to better control the jet breakup process. In this section we discuss the oscillation dynamics of a liquid jet subject to disturbances with wavenumbers larger than the cut-off wavenumber. The same parameters that have been considered for the jet breakup, namely $k$, $Re$, and $\epsilon_0$, are also considered here.

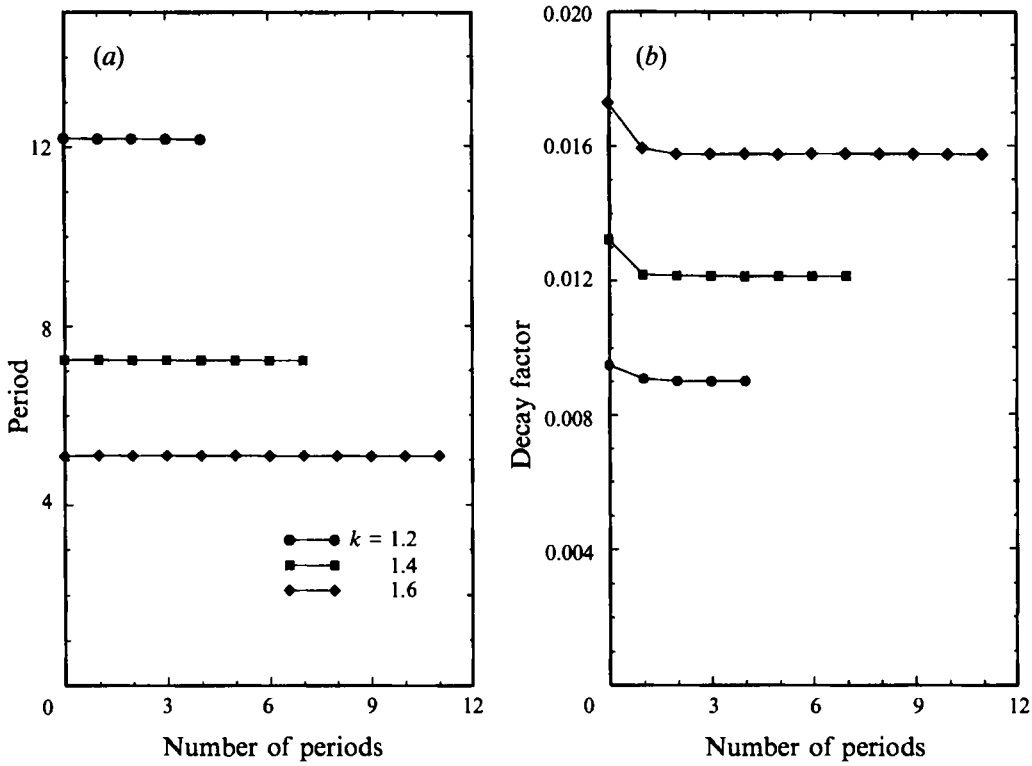


FIGURE 14. Time variation of (*a*) the period and (*b*) the decay factor for $Re = 200$ and $\epsilon_0 = 0.05$.

A capillary jet is stable for disturbances with $k > k_c$ and based on the linear theory it oscillates at a constant frequency. For a viscous jet the amplitude of the oscillation damps out and the jet eventually achieves an equilibrium cylindrical shape. The damping oscillations of a jet with $Re = 200$ subject to disturbance wavenumbers of $k = 1.2, 1.4$ and 1.6 and for a disturbance amplitude of 0.05 are considered. Figure 14(*a*) shows that the period of the oscillation stays relatively constant with time for different wavenumbers. Similarly, figure 14(*b*) shows that the decay factor, after an initially sharp drop, stays constant in time, and it increases with increasing the wavenumber. A physical explanation for the initially sudden drop in the decay factor can be given based on the part of the initial surface energy which is transformed into the kinetic energy at the end of the first period and which cannot be recovered as surface energy. Initially all the energy of the system is on the surface – there is no kinetic energy or basic state. Shortly after the onset of the fluid motion the surface energy is redistributed throughout the liquid in the form of kinetic energy. Since this transfer of energy is finite (not infinitesimal) and it is distributive, the recovery of all the kinetic energy into concentrated energy solely on the surface is not possible. Therefore, the jet surface amplitude will drop sharply at the end of the first period. In the subsequent periods the viscous damping will take effect and slowly reduce the amplitude with a constant decay factor. A mathematical explanation of the observed sudden drop in the decay factor can be given based on the Berger's (1988) initial-value analysis, in which a continuous spectrum of disturbances exist as $t \to 0$. For a stable jet, these disturbances, which have small amplitudes, damp out shortly after initiation, e.g. during the first period. Therefore, the overall effect appears as a sudden drop in the amplitude.

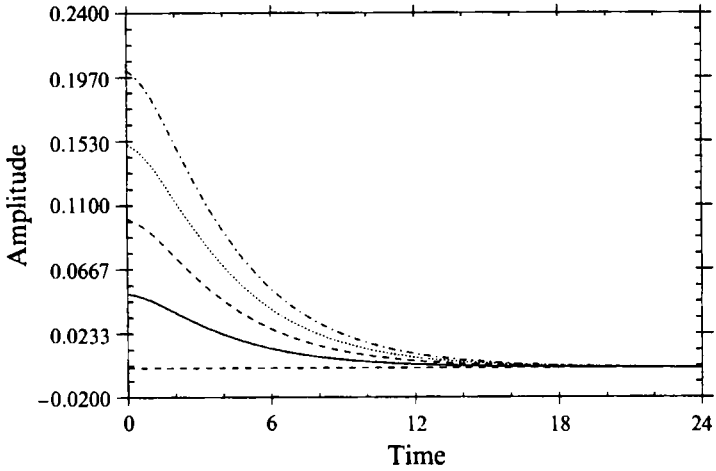


FIGURE 15. Effect of the amplitude of the initial disturbance on the overdamped oscillation of the difference between the radii of the swell and the neck points; $Re = 3.0$, $k = 1.2$: ——, $\epsilon_0 = 0.025$; – – –, $\epsilon_0 = 0.05$; · · ·, $\epsilon_0 = 0.075$; – · –, $\epsilon_0 = 0.1$.

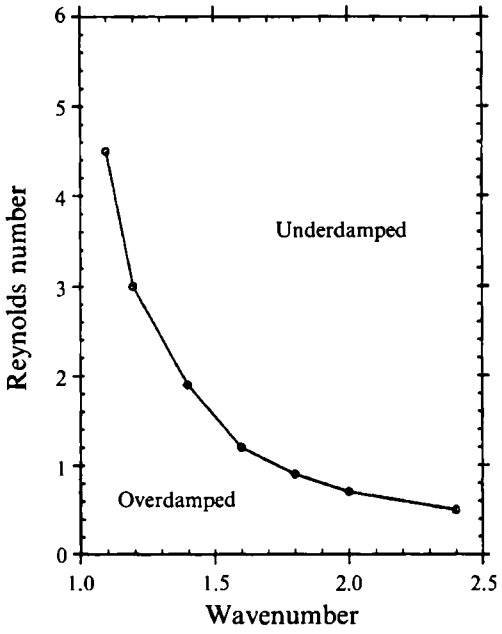


FIGURE 16. The boundary between the underdamped and overdamped oscillation in the $(Re, k)$-domain. $\epsilon_0 = 0.05$.

As $Re$ is reduced a value is reached below which the jet is overdamped and it does not oscillate. The effect of initial amplitude on overdamped oscillations is seen in figure 15. Increasing the initial amplitude of the disturbance to $\epsilon_0 = 0.1$ does not change the overdamped behaviour of the jet. However, it takes longer for the jet to come to rest. The regions of overdamped and underdamped oscillations have been calculated as a function of the Reynolds number and wavenumber for $\epsilon_0 = 0.05$ and are plotted in figure 16.

The influence of the initial disturbance amplitude on the oscillation of the jet is

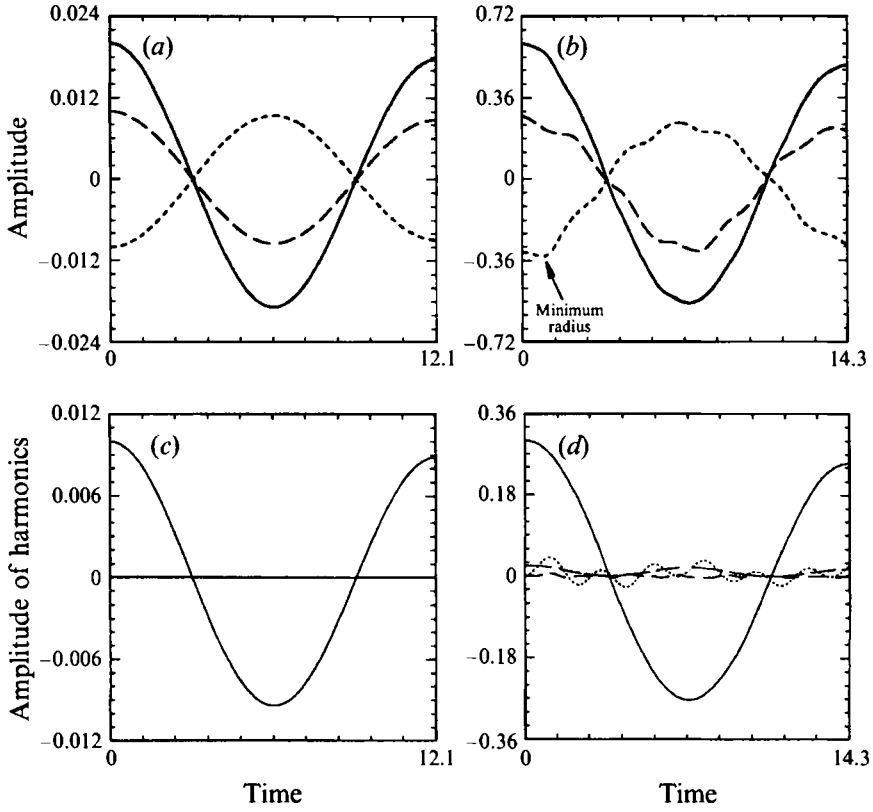


FIGURE 17. Amplitudes of swell (– –), neck (- - -), and their difference (——) as a function of time for $Re = 200$ and $k = 1.2$; (*a*) $\epsilon_0 = 0.01$, and (*b*) $\epsilon_0 = 0.3$. (*c*, *d*) The corresponding amplitudes of the fundamental (——), zeroth (— —), second (· · ·), and third (- - - -) harmonics as a function of time: (*c*) $\epsilon_0 = 0.01$, (*d*) $\epsilon_0 = 0.3$.

presented in figures 17(*a*) and 17(*b*) in terms of the amplitudes of the swell, neck, and their differences for a jet with $Re = 200$ and $k = 1.2$, and for initial amplitudes of $\epsilon_0 = 0.01$, and 0.3. For a very small amplitude of 0.01 the jet oscillates sinusoidally with gradual damping. As the amplitude increases the surface of the jet starts to deviate from the sine shape and reveals a secondary oscillatory behaviour superposed on the original disturbance. The nature of these secondary oscillations can be identified by plotting the fundamental and the higher harmonics of the surface with time, which are shown in figures 17(*c*) and 17(*d*). As discussed in §4.2, the higher harmonics are present right from the initiation. The amplitudes of these harmonics are small for small $\epsilon_0$; however, they progressively become larger with increasing $\epsilon_0$. This is clearly observed in figures 17(*c*) and 17(*d*). It is also noted that the observed secondary oscillations are mainly due to the second harmonic of the initial disturbance. The third harmonic does not appear until the initial amplitude of $\epsilon_0 = 0.4$. The same features are observed for low-*Re* jets except that the damping is more rapid. Figures 18(*a*) and 18(*b*) show the amplitude of the swell, neck and their difference as a function of time and for $Re = 30$ and 10, with $k = 1.2$ and for initial amplitude of $\epsilon_0 = 0.3$, with their surface harmonics in figures 18(*c*) and 18(*d*), respectively. Using the method of multiple timescales, Nayfeh (1970) showed that disturbances with $k > k_c$ oscillate with two frequencies, one being amplitude dependent, the other amplitude independent.

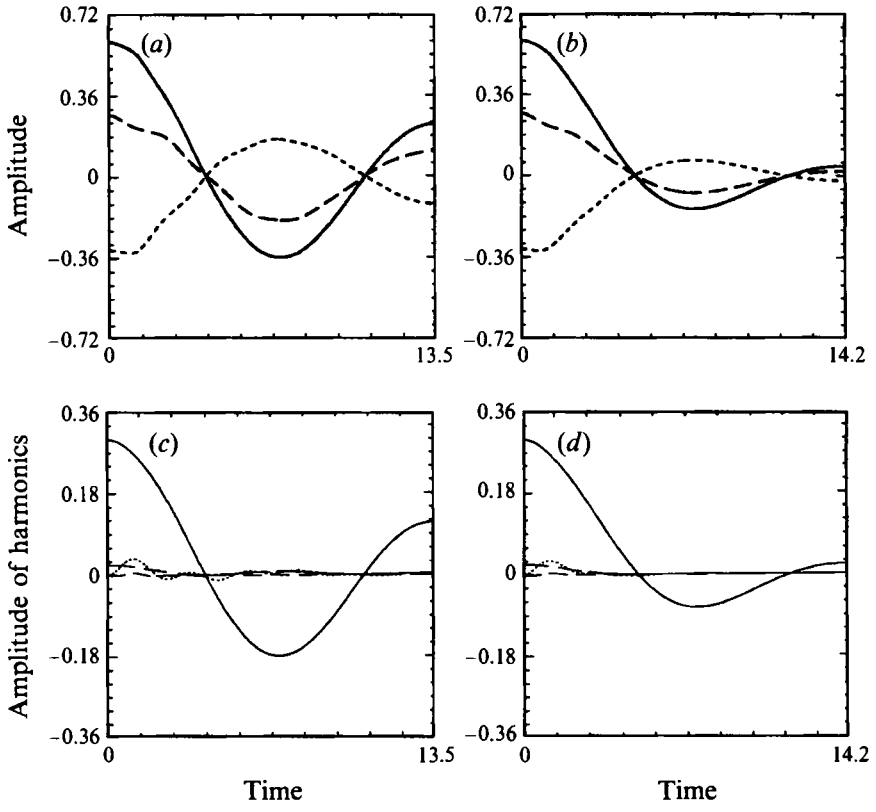


FIGURE 18. Amplitudes of swell (--), neck (---), and their difference (——) as a function of time for $k = 1.2$; $\epsilon_0 = 0.3$: (*a*) $Re = 30$, and (*b*) $Re = 10$. (*c*, *d*) The corresponding amplitudes of the fundamental (——), zeroth (— — —), second (· · ·), and third (— — —) harmonics as a function of time: (*c*) $Re = 30$, (*d*) $Re = 10$.

Interestingly, the high-*Re* jet of figure 17 shows similar behaviour. The fundamental frequency does not vary with the amplitude, yet the amplitude of the second harmonic is affected by the amplitude of the initial disturbance.

Study of the stable region ($k > k_c$) allows the investigation of the mechanism of transition from stable to unstable behaviour. The linear theory predicts a sinusoidal variation of the amplitude with time independent of the initial disturbance amplitude. However, the presence of nonlinear effects causes deviation from this smooth sinusoidal behaviour with increasing initial amplitude, as shown in figure 17(*b*). As the initial amplitude is increased, the contribution of higher harmonics, particularly the second harmonic, becomes more significant. The amplitude of the second harmonic increases with increasing initial amplitude. Eventually, an initial disturbance amplitude is reached at which the neck point first moves toward the axis, resembling the unstable behaviour of the jet. For the case shown in figure 17(*b*), the jet finally recovers the stable oscillation and the radius of the neck point increases with time, after passing through a minimum. (The minimum point is marked on the figure.) Further increases in the initial amplitude result in the attainment of a smaller minimum neck radius and eventually the neck point touches the axis before the jet finds the opportunity to reverse the downward motion. Therefore, the higher harmonics, in particular the second harmonic, play a major role in the transition from the stable to unstable region.

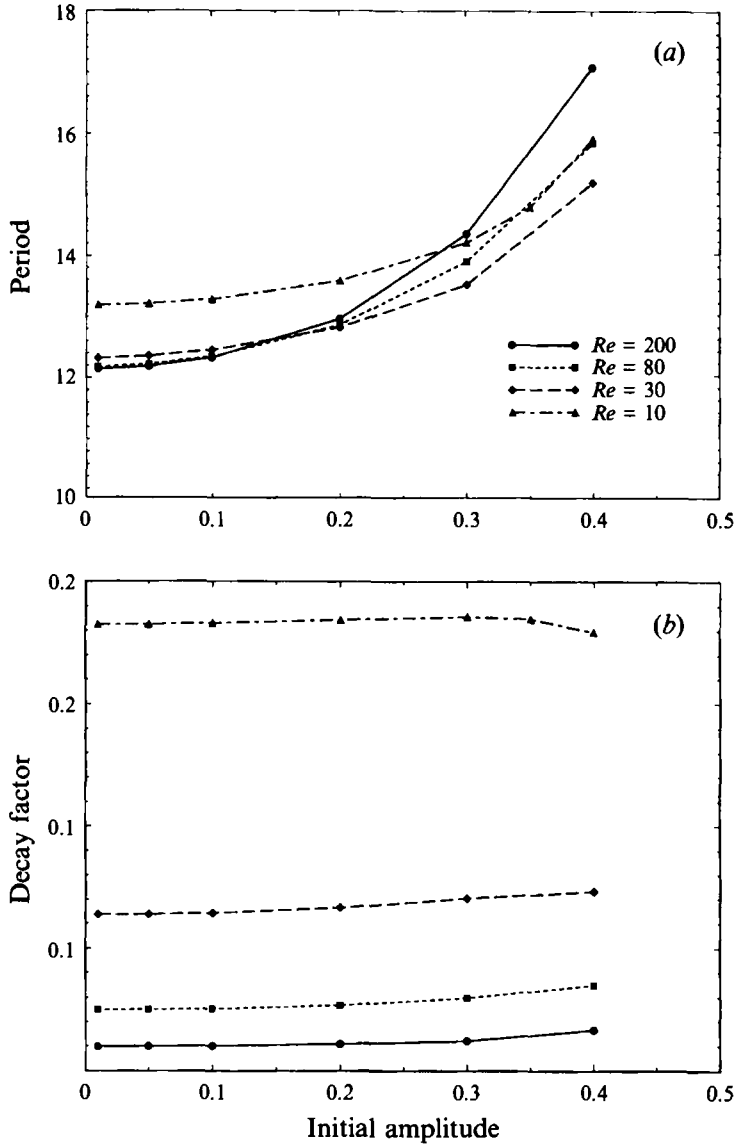


FIGURE 19. Variation of (*a*) the period of the oscillation and (*b*) the decay factor with the amplitude of the initial disturbance for various *Re* and for $k = 1.2$.

The effect of the initial disturbance amplitude on the period of the oscillation for different *Re* is shown in figure 19(*a*). Only the first period is considered. The first period always increases with the initial amplitude. At low amplitudes it decreases with increasing *Re*; however, at high amplitudes it increases with increasing *Re*. The damping rates of the amplitude for different *Re* and for various $\epsilon_0$ are plotted in figure 19(*b*). The results show that the damping rate increases with reducing *Re*, and it slightly increases with initial amplitude. At very large amplitudes and for lower *Re* the damping rate starts to decrease. When the amplitude is increased to $\epsilon_0 = 0.5$ the jet becomes unstable.

## 6. Conclusions

The problem of capillary jet breakup is investigated in the context of temporal instability. The Galerkin finite-element method is used along with the height-flux method for the advection and reconstruction of the free surface of the jet.

Based on the results obtained here the satellite drops are persistently formed after the breakup. Only for very small *Re* are the satellite drops not observed. Both the initial disturbance wavenumber and amplitude determine the *Re* below which no satellite is formed. We have provided the limiting *Re* for any given disturbance wavenumber and for initial disturbance amplitude of $\epsilon_0 = 0.05$, below which no satellites are observed (figure 9). An increase in the initial disturbance amplitude will shift the no-satellite region to higher *Re*. The results show that using jets with *Re* between 1 to 5 and disturbances with $k \geqslant 0.8$ the satellite formation can be prevented, even with very small initial disturbance amplitudes. An increase in amplitude also results in the reduction of the satellite size (figure 12). The results indicate that for an initial disturbance wavenumber of $k = 0.7$ and initial disturbance amplitudes up to 10% of the jet radius ($\epsilon_0 = 0.1$), the change in satellite size is not significant. However, there is a sharp drop in satellite size when $\epsilon_0$ is increased to about 20% of the jet radius, after which the satellite size does not change significantly. The results also indicate that the second harmonic of the fundamental disturbance is mainly responsible for the formation of the satellite drops. It is, therefore, expected that the satellite drop formation can be controlled by using frequency modulated disturbances. For instance, by disturbing the jet with two wavenumbers, one being the fundamental $k$, and the other being its second harmonic $2k$, one may be able to reduce the satellite size. This idea had been previously proposed and tested by Chaudhary & Maxworthy (1980*b*), Orme & Muntz (1990) and Bousfield *et al.* (1990) who have used a frequency- and/or amplitude-modulated initial disturbance to cause a more controlled breakup of the jet. Since for fundamental disturbance wavenumbers larger than 0.5 the higher harmonics are stable, the behaviour of the jet subject to stable wavenumbers is also investigated. The results show that the jet in the stable region may have underdamped or overdamped oscillations. The controlling parameters are *Re*, $k$ and $\epsilon_0$. For a small disturbance amplitude of $\epsilon_0 = 0.05$, the limiting *Re* (for a range of wavenumbers) below which the jet has overdamped oscillation is obtained (figure 16). Since for overdamped disturbances the amplitude continuously decreases in time, if the jet is disturbed such that the higher harmonics fall in the overdamped region, it is expected that the satellite size will become smaller.

This work was partially supported by the Fluid Mechanics Program of NSF under grant number CTS-9011201. Our thanks go to Dr M. L. Goldstein who initiated our interest in this topic, also to Professors Bousfield and Schulkes for reviewing our paper.

## REFERENCES

BERGER, S. A. 1988 Initial-value stability analysis of a liquid jet. *SIAM J. Appl. Maths* **48**, 973–991.

BIDONE, G. 1829 Experiences sur la forme et sur la direction des veines et des courants d'eau lances par diverses ouvertures. *Imprimerie Royale, Turin*, pp. 1–136.

BOGY, D. B. 1978*a* Use of one-dimensional Cosserat theory to study instability in a viscous liquid jet. *Phys. Fluids* **21**, 190–197.

BOGY, D. B. 1978*b* Wave propagation and instability of a circular semi-infinite liquid jet harmonically forced at the nozzle. *Trans. ASME* E: *J. Appl. Mech.* **45**, 469–474.

BOGY, D. B. 1979*a* Breakup of a liquid jet: Second perturbation solution for one-dimensional Cosserat theory. *IBM J. Res. Dev.* **23**, 87–91.

BOGY, D. B. 1979*b* Drop formation in a circular jet. *Ann. Rev. Fluid Mech.* **11**, 207–228.

BOUSFIELD, D. W., KEUNINGS, R., MARRUCCI, G. & DENN, M. M. 1986 Nonlinear analysis of the surface tension driven breakup of viscoelastic filaments. *J. Non-Newtonian Fluid Mech.* **21**, 79–97.

BOUSFIELD, D., STOCKEL, I. H. & NANIVADEKAR, C. K. 1990 The breakup of viscous jets with large velocity modulations. *J. Fluid Mech.* **218**, 601–617.

BOUSSINESQ, J. 1877 *Mem. Acad. Sci. Paris* **23**, 639.

CAULK, D. A. 1976 Some two and one dimensional problems in fluid mechanics by a direct approach. PhD thesis, University of California, Berkeley.

CAULK, D. A. & NAGHDI, P. M. 1977 The influence of twist on the motion of a straight elliptical jet. *University of California, Berkeley, Dept Mech. Engng Rep.* UCB/AM-77-5.

CAULK, D. A. & NAGHDI, P. M. 1978 The onset of breakup in inviscid and viscous jets. *University of California, Berkeley, Dept Mech. Engng Rep.* UCB/AM-78-3.

CHANDRASEKHAR, S. 1961 *Hydrodynamic and Hydromagnetic Stability*. Clarendon.

CHAUDHARY, K. C. 1977 Nonlinear capillary instability of a jet. PhD thesis, University of Southern California.

CHAUDHARY, K. C. & MAXWORTHY, T. 1980*a* The nonlinear capillary instability of a liquid jet. Part 2. Experiments on jet behavior before droplet formation. *J. Fluid Mech.* **96**, 275–286.

CHAUDHARY, K. C. & MAXWORTHY, T. 1980*b* The nonlinear capillary instability of a liquid jet. Part 3. Experiments on satellite drop formation and control. *J. Fluid Mech.* **96**, 287–297.

CHAUDHARY, K. C. & REDEKOPP, L. G. 1980 The nonlinear capillary instability of a liquid jet. Part 1. Theory. *J. Fluid Mech.* **96**, 257–274.

CHIN, R. H. 1983 Surface-tension-driven breakup of capillary jets of dilute polymer solutions. MS thesis, University of California, Berkeley.

CLINE, H. E. & ANTHONY, T. R. 1978 The effects of harmonics on the capillary instability of liquid jets. *J. Appl. Phys.* **49**, 3203–3208.

CRANE, L., BIRCH, S. & MCCORMACK, P. D. 1964 The effect of mechanical vibration on the breakup of a cylindrical water jet in air. *Brit. J. Appl. Phys.* **15**, 743–750.

DONNELLY, R. J. & GLABERSON, W. 1966 Experiment on capillary instability of a liquid jet. *Proc. R. Soc. Lond.* A **290**, 547–556.

FAIDLEY, R. & PANTON, R. L. 1990 Liquid jet instability induced by surface tension variations. *Expl Thermal. Fluid Sci.* **3**, 383–387.

FROMM, J. E. 1984 Numerical calculation of the fluid dynamics of drop-on-demand. *IBM J. Res. Dev.* **28**, 322–333.

GOEDDE, E. F. & YUEN, M. C. 1970 Experiments on liquid jet instability. *J. Fluid Mech.* **40**, 495–511.

GREEN, A. E. 1976 On the non-linear behavior of fluid jets. *Intl J. Engng Sci.* **14**, 49–63.

GREEN, A. E., NAGHDI, P. M. & WENNER, M. L. 1974 On the theory of rods. II. Developments by direct approach. *Proc. R. Soc. Lond.* A **337**, 485–507.

HUGHES, T. J. R., LIU, W. K. & BROOKS, A. 1979 Finite element analysis of incompressible viscous flows by penalty function formulation. *J. Comput. Phys.* **30**, 1–60.

KAKUTANI, T., INOUE, Y. & KAN, T. 1974 Nonlinear capillary waves on the surface of liquid column. *J. Phys. Soc. Japan* **37**, 529–538.

KELLER, J. B., RUBINOW, S. I. & TU, Y. O. 1973 Spatial instability of a jet. *Phys. Fluids* **16**, 2052–2055.

KEUNINGS, R. 1986 An algorithm for the simulation of transient viscoelastic flows with free surfaces. *J. Comput. Phys.* **62**, 199.

KITAMURA, Y., MISHIMA, H. & TAKAHASHI, T. 1982 Stability of jets in liquid–liquid systems. *Can. J. Chem. Engng* **60**, 723–731.

KITAMURA, Y. & TAKAHASHI, T. 1982 Breakup of jets in power law non-Newtonian–Newtonian liquid systems. *Can. J. Chem. Engng* **60**, 732–737.

LAFRANCE, P. 1975 Nonlinear break up of a laminar liquid jet. *Phys. Fluids* **18**, 428–432.

LEE, H. C. 1974 Drop formation in a liquid jet. *IBM J. Res. Dev.* **18**, 364–369.

LIEB, S. J. & GOLDSTEIN, M. L. 1986*a* The generation of capillary instabilities on liquid jet. *J. Fluid Mech.* **168**, 479–500.

LIEB, S. J. & GOLDSTEIN, M. L. 1986*b* Convective and absolute instability of a viscous liquid jet. *Phys. Fluids* **29**, 952–954.

MAGNUS, G. 1859 On the swellings formed in jets issuing from circular orifices. *Phil. Mag.* **18**, 161–183.

MANSOUR, N. N. & LUNDGREN, T. S. 1990 Satellite formation in capillary jet breakup. *Phys. Fluids* A **2**, 1141–1144.

MASHAYEK, F. & ASHGRIZ, N. 1993 A height flux method for simulating free surface flows and interfaces. *Intl J. Numer. Meth. Fluids* **17**, 1035–1054.

MCCARTHY, M. J. & MOLLOY, N. A. 1974 Review of stability of liquid jets and the influence of nozzle design. *Chem. Engng J.* **7**, 1–20.

NAYFEH, A. H. 1970 Nonlinear stability of a liquid jet. *Phys. Fluids* **13**, 841–847.

NAYFEH, A. H. & HASSAN, S. D. 1971 The method of multiple scales and nonlinear dispersive waves. *J. Fluid Mech.* **48**, 463.

OGG, J. C. & SCHETZ, J. A. 1984 Breakup and droplet formation of slurry jets. *AIAA J.* **23**, 432–439.

ORME, M. & MUNTZ, E. P. 1990 The manipulation of capillary stream breakup using amplitude-modulated disturbances: A pictorial and quantitative representation. *Phys. Fluids* A **2**, 1124–1140.

ORME, M., WILLIS, K. & NGUYEN, T.-V. 1993 Droplet patterns from capillary stream breakup. *Phys. Fluids* A **5**, 80–90.

PIMBLEY, W. T. 1976 Drop formation from a liquid jet: A linear one-dimensional analysis considered as a boundary value problem. *IBM J. Res. Dev.* **20**, 148–156.

PIMBLEY, W. T. & LEE, H. C. 1977 Satellite droplet formation in a liquid jet. *IBM J. Res. Dev.* **21**, 21–30.

PLATEAU, J. 1873 Statique experimentale et theorique des liquids soumis aux seules forces moleculaires. Cited by Lord Rayleigh, *Theory of Sound*, vol. II, p. 363, 1945. Dover.

RAYLEIGH, LORD 1879 On the instability of jets. *Proc. Lond. Math. Soc.* **10**, 4–13.

RAYLEIGH, LORD 1882 Further observations upon liquid jets. *Proc. Lond. Math. Soc.* **34**, 130–145.

RAYLEIGH, LORD 1896 *Theory of Sound*, vol. 2, 2nd edn. Macmillan. (Reprinted in 1945, Dover.)

RUTLAND, D. F. & JAMESON, G. J. 1970 Theoretical prediction of the sizes of drops formed in the breakup of capillary jets. *Chem. Engng Sci.* **25** (11-E), 1689–1698.

RUTLAND, D. F. & JAMESON, G. J. 1971 A non-linear effect in the capillary instability of liquid jets. *J. Fluid Mech.* **46**, 267–271.

SAVART, F. 1883 Memoire sur la constitution des veines liquides lancees par des orifices circulaires en mince paroi. *Ann. Chimie Phys.* **53**, 337–386.

SCHULKES, R. M. S. M. 1993 Dynamics of liquid jets revisited. *J. Fluid Mech.* **250**, 635–650.

SHOKOOHI, F. & ELROD, H. G. 1987 Numerical investigation of the disintegration of liquid jets. *J. Comput. Phys.* **71**, 324–342.

SMITH, S. W. J. & MOSS, H. 1917 Experiments with mercury jets. *Proc. R. Soc. Lond.* A **93**, 373–393.

TAUB, H. H. 1976 Investigation of non-linear waves on liquid jets. *Phys. Fluids* **19**, 1124–1129.

TJAHJADI, M., STONE, H. A. & OTTINO, J. M. 1992 Satellite and subsatellite formation in capillary breakup. *J. Fluid Mech.* **243**, 297–317.

TORPEY, P. A. 1989 A nonlinear theory for describing the propagation of disturbances on a capillary jet. *Phys. Fluids* A **1**, 661–671.

TYLER, E. 1933 Instability of liquid jets. *Phil. Mag.* **16**, 504–518.

TYLER, E. & WATKIN, F. 1932 Experiments with capillary jets. *Phil. Mag.* **16**, 849–881.

VASSALLO, P. & ASHGRIZ, N. 1991 Satellite formation and merging in liquid jet breakup. *Proc. R. Soc. Lond.* A **433**, 269–286.

WANG, D. P. 1968 Finite amplitude effect on the stability of a jet of circular cross-section. *J. Fluid Mech.* **34**, 299–313.

WEBER, C. 1931 Zum Zerfall eines Flussigkeitsstrahles. *Z. Angew. Math. Mech.* **11**, 136–141.

YUEN, M. C. 1968 Non-linear capillary instability of a liquid jet. *J. Fluid Mech.* **33**, 151–163.